Hindawi
Advances in Materials Science and Engineering
Volume 2018, Article ID 8979678, 10 pages
https://doi.org/10.1155/2018/8979678

Research Article

Microstructure and Wear Resistance of TIG Remelted NiCrBSi Thick Coatings

Guo-lu Li,[1] Ya-long Li,[1,2] Tian-shun Dong,[1] Hai-dou Wang,[2] Xiao-dong Zheng,[1,2] and Xiu-kai Zhou[1]

[1]*School of Materials Science and Engineering, Hebei University of Technology, Tianjin 300130, China*
[2]*National Key Laboratory for Remanufacturing, Academy of Armored Forces Engineering, Beijing 100072, China*

Correspondence should be addressed to Tian-shun Dong; dongtianshun111@163.com

Received 30 November 2017; Accepted 18 February 2018; Published 21 March 2018

Academic Editor: Shuo Yin

The self-fluxing NiCrBSi coatings with 800 μm thickness were prepared on the surface of AISI1045 steel substrate by plasma spraying. And the remelted coating was obtained using by the tungsten inert gas (TIG) arc process. The microstructure, surface roughness, hardness, phase composition, and wear resistance of the sprayed coating and remelted coating were systematically investigated. The results demonstrate that TIG remelted treatment can significantly eliminate the microscopic defects in thick coating and improve its density. The surface roughness (Ra) of the remelted coating is only 18.9% of the sprayed coating. The hardness of the remelted coating is 26.8% higher than that of the sprayed coating. The main phases in the sprayed coating are changed from γ-Ni, Cr_7C_3, and Cr_2B to γ-Ni, $Cr_{23}C_6$, CrB, Ni_3B, and Fe_3C. The wear mass loss of the remelted coating is only 17.1% of the sprayed coating. Therefore, a Ni-based thick coating with good wear resistance can be obtained by plasma spraying and remelted technique.

1. Introduction

Because of their high ability to withstand extremes of temperature, excellent wear resistance, and high corrosion properties, Ni-based self-fluxing alloy coating has been widely used in petroleum, chemical, power, defense, and other fields [1–3]. At present, Ni-based self-fluxing alloy coating is mainly prepared by flame spraying and plasma spraying. However, the abovementioned methods are quite prone to produce microdefects within the coating, such as delamination, micropores, cracks, and so on. These microdefects reduce its density and the bonding strength between the coating and the metal substrate, which results in the decrease of the life of coating. In addition, some studies have shown that the thick coating has better wear resistance and fatigue properties than the thin coating within a certain range [4, 5]. However, thick coating is likely to peel from the substrate during the preparation process due to the large internal stress and other factors [6, 7]. Therefore, thick coating is difficult to be applied in production practice.

Some studies have proved that the thin coating can be surface modified and strengthened by remelting to eliminate the layer structure of coating, reduce the porosity, and improve the interface bonding with the substrate [8], which are beneficial for improving the coating's performance [9] and prolonging the service life of the parts [10–12]. Unfortunately, little attention has been paid to the remelted of thick coatings.

In the present work, the NiCrBSi coating with the thickness of 800 μm was prepared on the AISI1045 substrate by plasma spraying. And the thick remelting coating was produced by tungsten inert gas (TIG) arc process. The microstructure, morphology evolution, the friction, and wear properties of coating before and after remelting were systematically analyzed. The purpose of this research is to produce the thick coating and improve the service life of the coating.

2. Experimental Procedure

The substrate selected is AISI1045 steel with a size of 10 mm × 10 mm × 10 mm. The sprayed raw material is a commercial NiCrBSi self-fluxing alloy powder with a particle size of 10 μm~60 μm, and the chemical composition is given in Table 1.

The powder was preheated, and the substrate AISI1045 steel was cleaned and grit-blasting before spraying. The coating with the average thickness of 800 μm was prepared by using the BT-G3 plasma spraying system with compressed air as main and powder feeding gas. The sprayed coating was remelted by the TIG method with YC-300WX welding machine. Process parameters of sand blasting, spraying, and remelting are given in Table 2.

The microstructures and compositions of the coatings were analyzed by Hitachi S4800 field emission scanning electron microscope (SEM) equipped with an energy dispersive X-ray spectrometer (EDS). The phase identification of the samples before and after remelting was conducted by a D/max/2500 PC type X-ray diffractometer with monochromatic Cu Kα radiation. The tube voltage and current were 40 kV and 150 mA, respectively, and the scanning speed and range were chosen 3°/min and 20°~90°, respectively. The microhardness was evaluated on a Shimadzu HMV-2000 Vickers hardness tester.

The wear resistance test was carried out on UMT-2 multifunction friction and wear tester. The diameter of the GCr15 ball was 4 mm, and its Rockwell hardness was 61 HRC. In order to ensure the consistence of the experimental conditions, the samples were grinded with SiC sandpaper from #400 to #1000 before the experiment, until the surface roughness (Ra) of the sample was less than 0.8 μm, and then polished. Experimental conditions were as follows: load 30 N; frequency 10 Hz; test duration 20 min; amplitude 4 mm; and room temperature. The surface roughness, the three-dimensional morphology, and the wear mass loss of the coatings after wear testing were measured by the Phase Shift MicroXAM-3D topography instrument.

Table 1: Chemical composition of NiCrBSi powder.

Element	Cr	B	Si	Mn	Re	Ni
wt. %	17	2.5	3	2	0.5	Bal.

Table 2: Grit-blasting, spraying, and remelting process parameters.

Process	Parameters	Values
Grit blasting	Air pressure (MPa)	0.7
	Blasting distance (mm)	300
	Blasting angle (°)	90
Plasma spraying	Voltage (V)	60
	Current (A)	500
	Spraying distance (mm)	150
	Cooling of substrate	Air blow
	Gas flow rate (L/min)	Ar(80) H_2(130)
	Coating thickness (mm)	0.80
TIG remelting	Current (A)	90
	Arc length (mm)	2
	Argon flow (L·min^{-1})	10
	Scanning speed (mm·min^{-1})	150
	Step size (mm)	3

3. Results and Discussion

3.1. Microstructure. Figure 1 shows the morphology of the sprayed coating. It can be seen that a typical mechanical bonding has formed between the coating and the substrate from Figure 1(a). There are many inclusions, voids, unmelted particles, and microcracks in the coating, and the interface between the coating and the substrate is nonuniform. The flattening degree of particles varies when they hit the substrate continuously during the spraying process due to the heating and acceleration action of flame flow on the powder is different. The coating presents a typical lamellar structure, consisting of flat striped and spherical particles, and a distinct interface or crack forms. As shown in Figure 1(b), the length of the strip particles is 10.1 μm~45.6 μm; the thickness is 1.5 μm~9.8 μm; and the particle diameter is 5.1 μm~25.2 μm. The porosity of the coating measured by image processing software Image J2x is 5.6%.

The cross-sectional morphology of the remelted coating is shown in Figure 2(a). After remelting, the lamellar structure of the original coating disappears. The interface between coating and substrate is smooth, and there are no obvious microcracks, voids, and other defects inside the coating. Figure 2(b) shows that the remelted coating has a bright area of 4.5 μm thickness at the bottom of the coating. The porosity of the remelted coating measured with Image J2x software is 0.2%, which indicates that the density has been improved remarkably. At the interface of the coating, the lamellar structure disappears, and the columnar crystal grows with the recrystallization phenomenon, which helps to improve the interface bonding strength.

The EDS analysis is performed by selecting 6 points in the vertical direction of the interface from the substrate to the sprayed coating. Point 1 and point 2 are located in the substrate, and point 3 is located in the interface between the substrate and the coating. Points 4, 5, and 6 are located in the coating. EDS spectrum analysis shows that the main component of point A in Figure 1(b) is atom fraction: 46.99% O, 1.50% Si, 15.75% Cr, and 35.75% Ni, which indicates that point A is oxidized inclusion.

The EDS analysis is performed on 6 points near the interface between the remelted coating and the substrate. The point 1 and point 2 are located in the substrate. The atomic radii of B and C elements are small, and the concentration gradient is large at the interface; hence, they are able to diffuse into the substrate for a long distance. Although the concentration gradient of the Ni element at the interface is also high, its atomic radius is large; hence, its diffusion distance is short in the substrate. Point 3 is located in the bright area, where the contents of Ni and Cr element are higher, and B and C elements are enriched; since the activities of B and C elements are very high, B and C are easy to form compounds with Cr and Ni. Points 4, 5, and 6 are located inside the remelted coating, so the remelted coating contains a small amount of Cr, Si, and B elements which dissolves in γ-Ni solid solution. In addition, the remelted coating also contains more iron, which is due to a small amount of substrate was remelted and went into the remelted coating. Under the action of stirring of the arc force [13], Fe atoms were distributed roughly uniformly in the remelted coating.

In order to understand the interface bonding between the coating or remelted coating and the substrate more

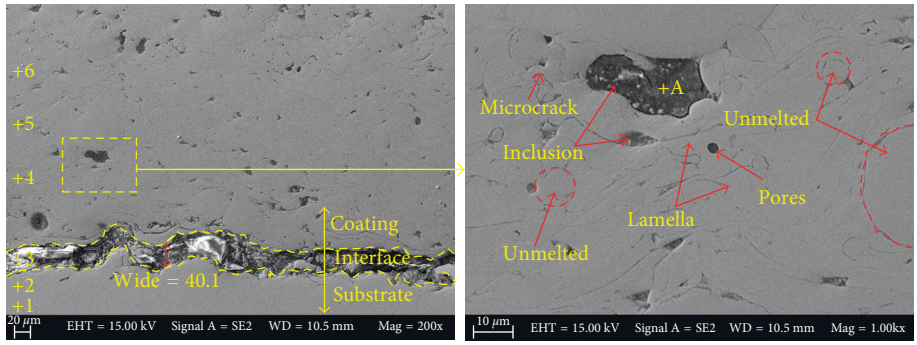

(a) (b)

Figure 1: SEM morphology of sprayed coating: (a) low magnification and (b) high magnification.

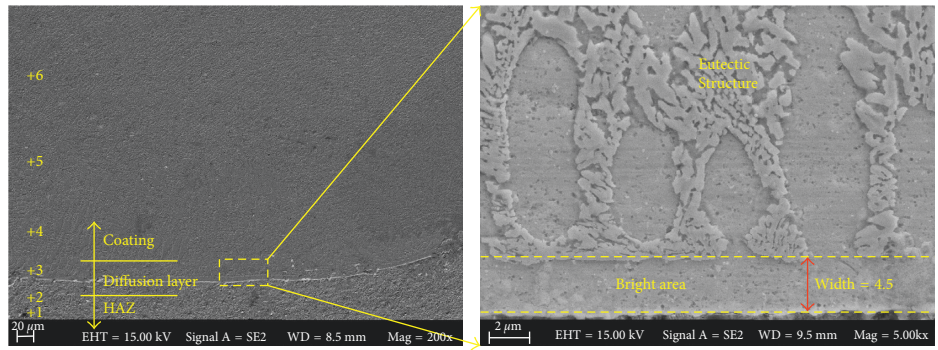

(a) (b)

Figure 2: SEM morphology of remelted coating cross section: (a) low magnification and (b) high magnification.

clearly, the element distribution of the interface was detected by line scanning, as shown in Figure 3. Compared with the sprayed coating, the elements of Fe, Ni, Cr, B, and Si at the interface of remelted coating have a certain gradient. This indicates that the dissolution and diffusion of elements between the two sides of the interface have occurred which is caused by the concentration and temperature gradients during the remelting process.

The first law of diffusion can be described as follows:

$$J = -D\frac{dc}{dx}, \tag{1}$$

where D is the diffusion coefficient. Besides the temperature and diffusion time, the diffusion of element is also affected by the element diffusion coefficient D and the concentration gradient dc/dx.

The concentration gradients of Fe and Ni at the interface of substrate AISI1045 steel and NiCrBSi coating are very large, which would help to accelerate diffusion, while the C and B elements have a small atomic radius, which is also beneficial for diffusion. The EDS line scanning of interface of the sprayed coating and the substrate is shown in Figure 3(a). It is obviously seen that Fe, Ni, Cr, B, and C elements are steep changes, indicating that there is no diffusion between each other. The coating and the substrate only belongs to mechanical bonding. The EDS line scanning of the interface of the remelted coating and the substrate is shown in Figure 3(b). Obviously, diffusion of Fe, Ni, Cr, B, and C elements occurred at the interface. The combination of remelted coating and substrate belongs to metallurgical bonding.

The XRD spectra of NiCrBSi powder, sprayed coating, remelted coating bottom, and remelted coating surface are shown in Figure 4. It can be seen that the main phases of the powder are γ-Ni, Cr_7C_3, Cr_2B, CrB, and Ni_3B; the main phases of the coating are γ-Ni, Cr_7C_3, and Cr_2B; the surface of the remelted coating are γ-Ni, Cr_7C_3, $Cr_{23}C_6$, and CrB; and the bottom phases of the remelted coating are γ-Ni, $Cr_{23}C_6$, CrB, Ni_3B, and Fe_3C. Therefore, the remelted coating has more new strengthening phases, such as $Cr_{23}C_6$, CrB, Ni_3B, and Fe_3C.

The sprayed coating and a few substrates are melted to form molten pool under the influence of the arc heat. After the arc is removed, the molten pool solidifies. The growth diagram of the interface microstructure of the remelted coating during the solidification process is shown in Figure 5. The bonding layer between the remelted coating and substrate has grown in form of plane crystal and then grown away from the interface in the form of dendrites. The microstructure of remelted coating is obviously different among the interface layer, the middle of remelted coating, and the top. The remelted coating is combined with the substrate to form a bright area. The middle part is dendrites, and the upper part is smaller dendrites whose microstructure is relatively fine. The microstructures of the central and the top parts are having little difference, and the direction of dendrite growth is in a certain angle with the interface. In

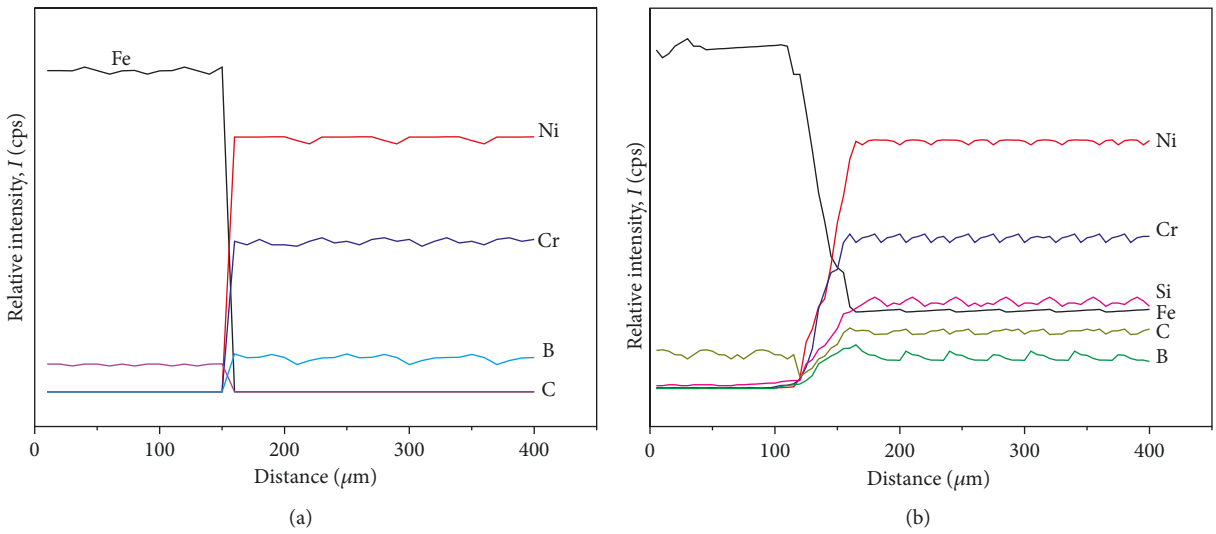

Figure 3: Element distributions along thickness of the sprayed and remelted coating: (a) sprayed coating and (b) remelted coating.

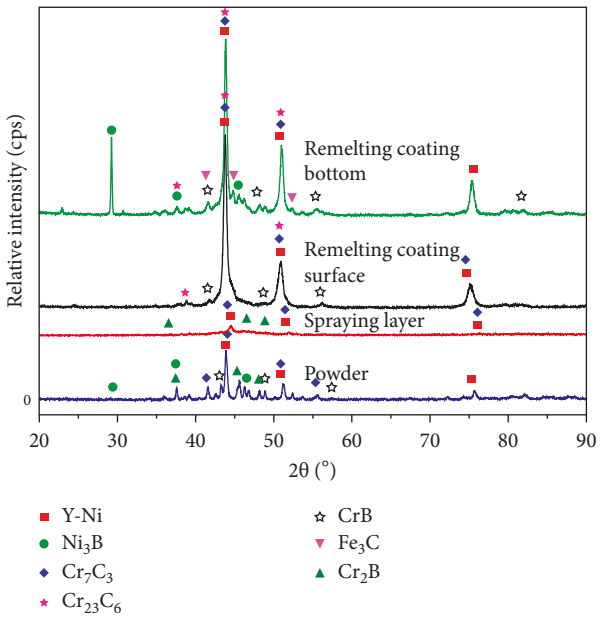

Figure 4: XRD patterns of powder, sprayed coating, and remelted coating.

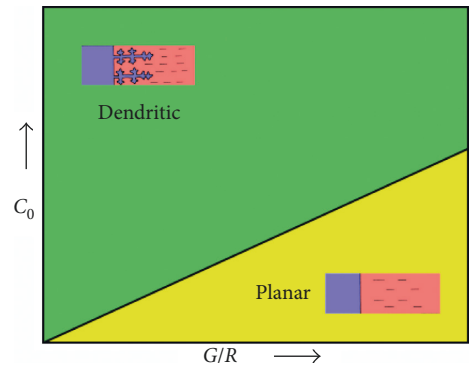

Figure 5: Crystal growth patterns of different components undercooled.

remelted coating, dendrite growth is not only controlled by heat flow direction, but also affected by molten pool disturbance and crystalline anisotropy. Therefore, the growth direction of the dendrite structure shows a certain angle with the normal interface of the solid-liquid interface.

According to the principle of solidification kinetics [14, 15], the crystallization process of the liquid phase is driven by the force of the phase transformation and then overcomes the energy barrier with the help of energy fluctuation, so the crystallization is realized by nucleation and growth. The new phases $Cr_{23}C_6$, CrB, Ni_3B, and Fe_3C formed in the remelted coating can be used as nucleus, and the agitation in the remelting process makes the microstructure more refined. The overall microstructure of the remelted coating is shown in Figure 6(a). Figures 6(b)–6(d) are local (B, C, and D) amplification of Figure 6(a), respectively. The main influence factors of the crystalline morphology of the TIG remelted coating are the liquid phase composition in the molten pool and the shape control factor K [14]. The shape control factor is expressed as follows:

$$K = \frac{G}{R}, \tag{2}$$

where G is the temperature gradient of the interface of liquid-solid and R is the interface moving speed. The interface morphology of liquid-solid of the remelted coating mainly depends on the size of the G/R ratio. The solidification velocity R tends to zero at the bottom of the molten pool, and G is very large [14]. Therefore, K has a very large value, where the solidified structure grows at a low velocity plane to form a planar crystal, which is called "bright area," as shown in Figure 6(b). The width of bright area is 4.5 μm (Figure 2(b)). With the increase of the distance from the binding interface, the solidification rate R increases [14]; hence, K decreases, which is beneficial to dendrites formation, as shown in Figures 6(c) and 6(d).

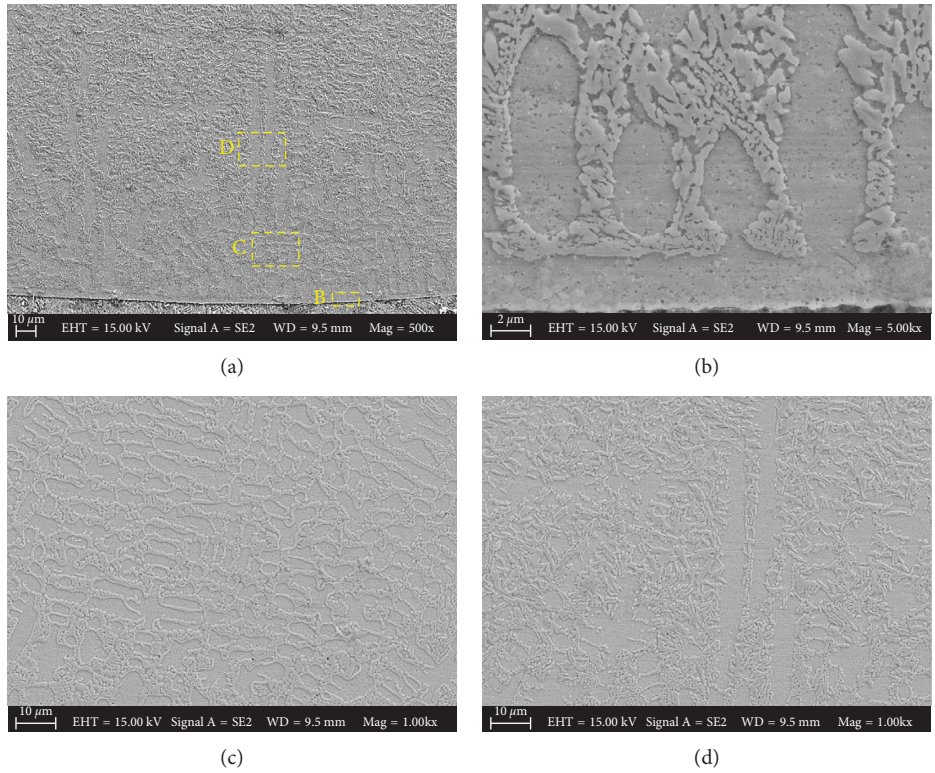

(a) (b) (c) (d)

Figure 6: Microstructure and morphology of remelted coating: (a) overall structure, (b) planar crystal, and (c, d) dendritic crystal.

In fact, the bright area is planar crystal. As shown in Figure 2(b), the width of bright area is 4.5 μm, which is often considered as feature of metallurgical bonding. In addition, because of the good corrosion resistance of the bright area, it can be displayed in the form of the bright area. From the element distributions along thickness of the remelted coating in Figure 3 and XRD of the remelted coating in Figure 4, the bright area is γ-Ni, in which a small amount of Fe and Cr elements are dissolved.

The eutectic structures of the remelted coating are shown in Figures 7(a) and 7(b), and EDS results of point E and point F are shown in Figures 7(c) and 7(d). The eutectic structure consists of gray strip γ and black γ'. According to the XRD results presented in Figure 4, it can be determined that the gray strip γ is γ-(Fe, Ni, and Cr), where a small amount of carbon gets into the lattice gap and leads to lattice deformation, and the black γ' are hard phases formed of $Cr_{23}C_6$, CrB, Ni_3B, and Fe_3C.

3.2. Surface Roughness. The three-dimensional morphology of the surface of the sprayed coating and the remelted coating is shown in Figures 8(a) and 8(b). The maximum roughness Rz max, minimum roughness Rz min, and average roughness Ra of the sprayed and remelted coating are shown in Table 3. It is obviously seen that Ra of the surface of the remelted coating is only 18.9% of the sprayed coating. In fact, the surface quality of remelted coating obtained by this experiment is better than that of vacuum remelting, and Ra of the TIG remelted coating is 25.2% compared with the vacuum remelted coating [16]. This fully demonstrates that the TIG remelted coating makes the surface roughness of the sprayed coating significantly reduce.

Previous literatures showed that the size and number of defects in the coating affected the roughness [17, 18]. In this study, there are many defects inside the sprayed coating, such as unmelted particles, voids, inclusions, and so on, which can increase the coating surface roughness. After TIG remelting treatment, the unmelted particles are remelted, most of the pores are eliminated, and the state and distribution of the particles are more homogeneous compared with the sprayed coating. As a result, the surface roughness is greatly decreased.

3.3. Hardness. Figure 9 shows the hardness change curve on the cross section of the sprayed coating and remelted coating. It can be seen that the hardness of the two coatings are all remarkably higher than that of AISI1045 steel substrate, whose hardness is 300 $HV_{0.1}$. The average hardness of the remelted coating (900 $HV_{0.1}$) is higher than that of sprayed coating (710 $HV_{0.1}$). The hardness of the remelted coating is about 26.8% higher than that of the sprayed coating. Moreover, the fluctuation of the hardness of coating is greater. The reasons are as follows:

(1) The internal structure of the sprayed coating is loose, which reduces hardness of the coating. However, the convection and the stirring effect of arc on the molten pool during the remelting process causes gas escaping from the molten pool [19–22]. Meanwhile, due to the deoxidation role of Si and Mn in the

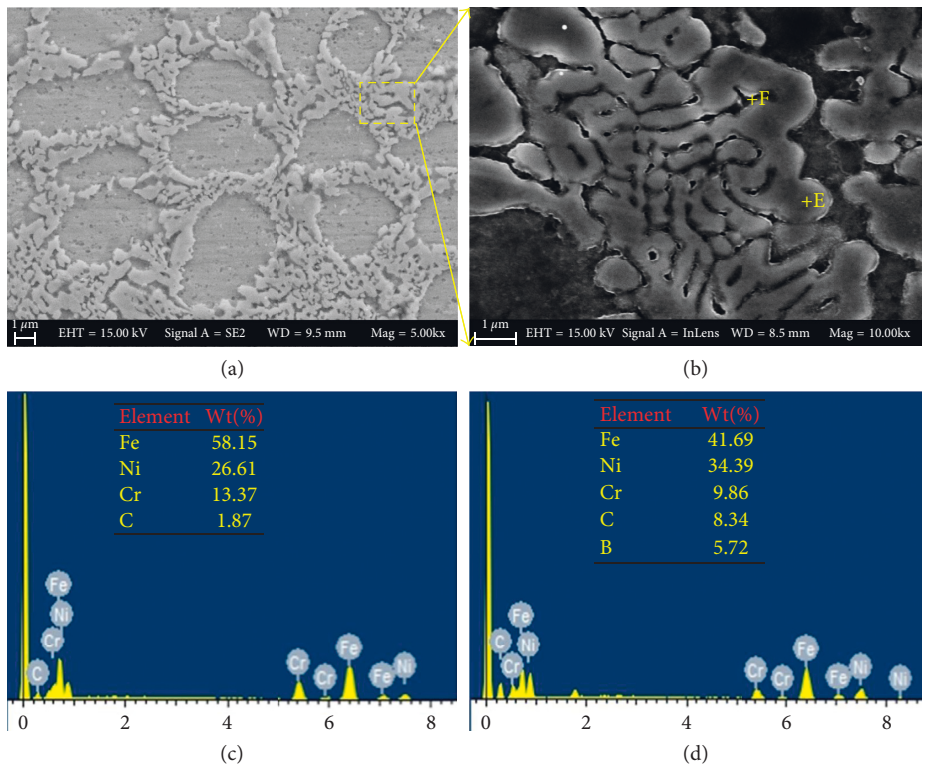

Figure 7: Eutectic structure and the energy spectrum and weight percentage of point E and point F.

molten pool, the oxidation inclusions can be removed effectively. Therefore, the microstructure of the remelted coating has become more compact and uniform, and its hardness is increased.

(2) Although there are some hard phases, such as Cr_7C_3 and Cr_2B, and a part of unmelted or semimelting particles in the sprayed coating, the research by Ohmori et al. shows that the interfacial bonding area of sprayed coating is generally less than 1/3 of the total interface and 2/3 or more is the unbound interface, which are unfavourable for the hardness [23]. However, after the remelting, the microstructure of remelting coating becomes more compact and uniform, a large number of dispersed carbides formed, and the harden phases such as fine skeleton like Ni_3B, CrB, and $Cr_{23}C_6$ disperse evenly in γ-Ni, which makes the hardness of remelted coating increase and uniform.

In addition, it is necessary to point out that there is significant transition zone between the hardness of the remelted coating and the substrate, and there is no obvious transition zone between the sprayed coating and the substrate. This is because Ni and Cr in the coating have diffused into the substrate during the remelting process, leading to the formation of some hard phases such as $Cr_{23}C_6$ and CrB. At the same time, Ni and Cr can increase the hardenability of substrate. In fact, such transition zone is beneficial for the interface bonding between the remelted coating and the substrate. This phenomenon also confirms the bonding between the coating and the substrate is a typical mechanical combination, whereas the bonding between the remelted coating and the substrate is a typical metallurgical combination.

3.4. Wear Resistance. Figure 10 shows the friction coefficient curve of the sprayed and remelted coating. 0~100 s is the fluctuating stage, and 100~1200 s is the stable wearing stage. The average coefficient of friction of the sprayed coating is 0.551, while the average coefficient of friction of the remelted coating is 0.392. It is evident that the friction coefficient and the range of fluctuation of sprayed coating are larger than that of remelted coating.

The 3D topography of the wear scar of two coatings is shown in Figures 11(a) and 11(b). At room temperature, the width and depth of wear scar of the sprayed coating are larger than that of the remelted coating. According to Figure 12(a), the widths of the wear scar of the sprayed and remelted coating are 1.132 mm and 0.5132 mm, respectively, and the depths of wear scar are 26.79 mm and 10.03 mm, respectively. The wear mass losses of the sprayed and remelted coating are measured by 3D profilometer, as seen in Figure 12(b). The wear mass losses of the sprayed and remelted coating are 0.2102 mm^3 and 0.0357 mm^3, respectively, and the latter is only 17.1% of the former. Therefore, the wear property of remelted coating has been significantly improved after remelting.

The SEM morphology of surface wear of the sprayed coating is shown in Figure 13(a). Its local magnification is shown in Figure 13(b). It can be seen that the surface of the sprayed coating shows spalling and delamination. The

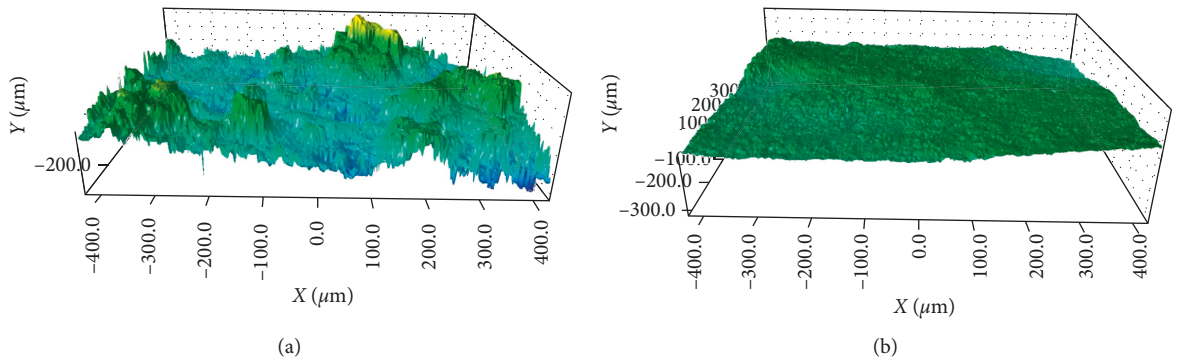

Figure 8: 3D morphologies of coatings obtained by a laser scanning microscope: (a) sprayed coating and (b) TIG remelted coating.

Table 3: Surface roughness of spraying and remelting coating.

	Rz max (μm)	Rz min (μm)	Ra ave (μm)
Plasma spraying	266.936	202.416	12.651
Vacuum remelted coating [16]	143.841	139.739	9.512
TIG remelted	31.239	28.836	2.403

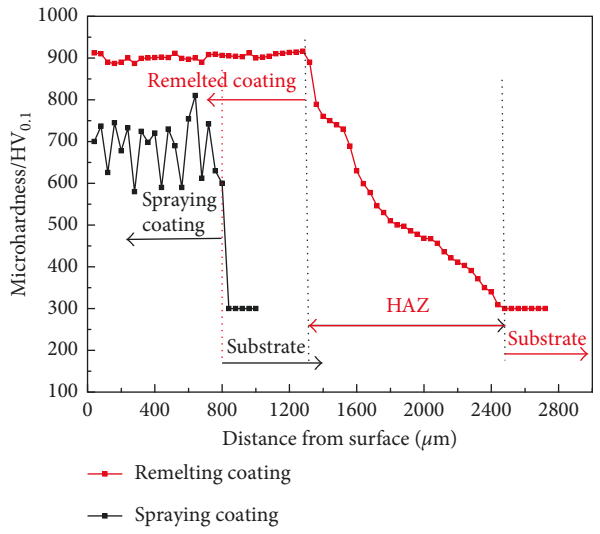

Figure 9: Microhardness of sprayed and remelted coating.

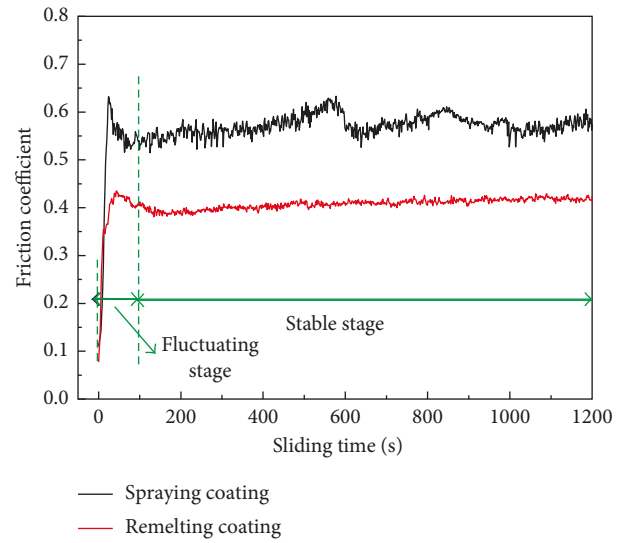

Figure 10: The friction coefficient curve of the sprayed and remelted coating.

spalling phenomenon of the coating is serious, and there are many spalling pits, where some microcracks, pores, and unmelted particles of 20 μm~50 μm can be found. In addition, the spalling pits are filled with lots of strip debris, whose diameters are 1 μm~2.5 μm (Figure 13(c)), and the oxygen content is high, together with a small amount of Si element (Figure 13(d)). Therefore, the wear mechanism of the coating is mainly lamellar cracking and oxidation wear.

The SEM morphology of surface wear of the remelted coating is shown in Figure 14(a). There are some furrows on the surface of the remelted coating (Figure 14(b)). The furrows are filled with lots of debris, whose shapes are fine granular and its diameter is 0.5 μm~0.8 μm (Figure 14(c)), and the oxygen content is high (Figure 14(d)). Therefore, the wear mechanism of remelted coating is mainly micro-abrasive wear and oxidation wear.

The reasons for the improvement of wear resistance of remelted coating are as follows:

(1) There are many inherent microcracks in the sprayed coating, and they are likely to extend in the wear process under the alternating load, which lead to the spalling eventually (Figure 13(b)). While for the remelted coating, TIG remelted eliminates the inherent defects of the coating and improves the wear resistance of the remelted coating accordingly.

(2) From the point of view of phase change, according to the theory of Colaco, *R* [24],

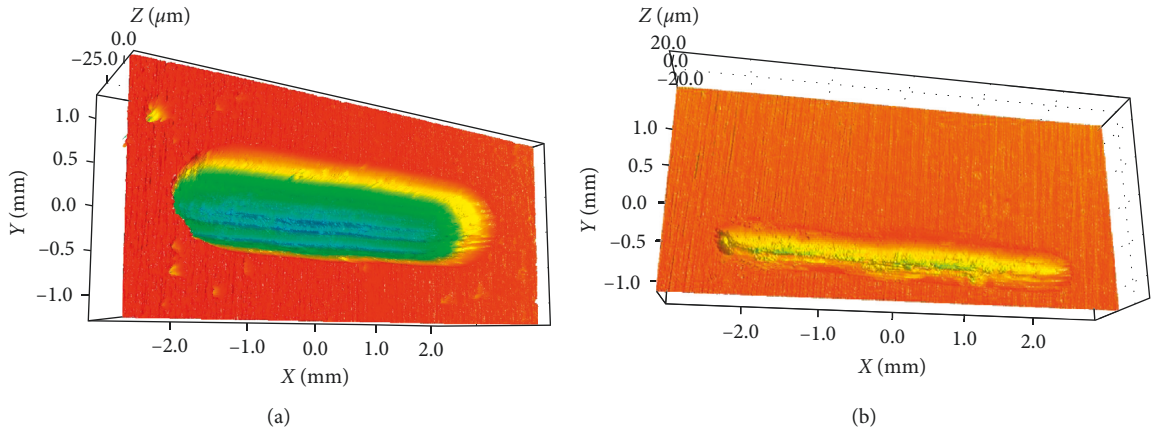

Figure 11: Three-dimensional morphology of worn track: (a) sprayed coating and (b) remelted coating.

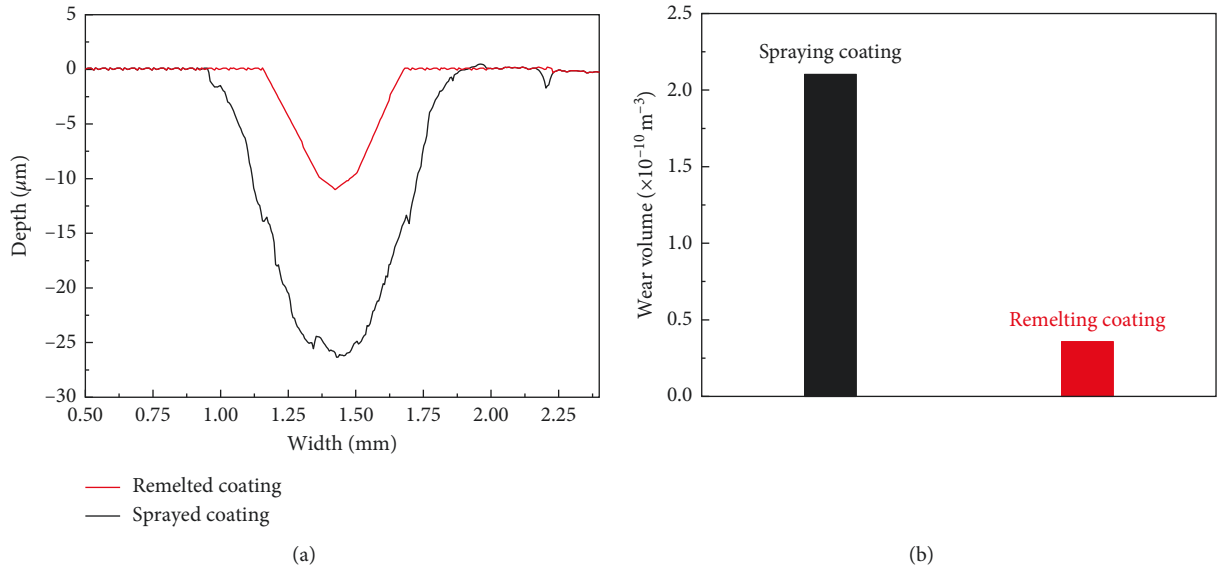

Figure 12: (a) Outline of wear scar of sprayed and TIG-remelted coatings and (b) wear mass loss.

$$Q' = K' d^3 \sqrt{\frac{H_0}{x^2} + \frac{\beta}{x}} + \lambda' \left[\frac{32 F_N}{\pi \tan^2 \varphi} + \frac{x^2}{H_0 + \beta x} \right]^{1/2}, \quad (3)$$

where Q' is the wear rate, K' is the wear coefficient, d is the particle diameter, H_0 is the hardness of the coating, x is the hard reinforced particle volume fraction, β is constant, λ' is the probability of hard particles pulled out of the wear surface, F_N is the load of abrasive grains, and φ is the angle of tapered abrasive grains. In this work, the main factors affecting the wear resistance of the coating are the particle diameter of hard particles (d), hard reinforced particle volume fraction (x), and the probability of hard particles pulled out of the wear surface (λ').

Compared with the sprayed coating, the remelted coating produces more dispersed fine skeleton-like $Cr_{23}C_6$, CrB, and Ni_3B phases which indicates that hard reinforced particle volume fraction (x) is higher and the average diameter of these hard particles (d) are smaller than that of the spraying coating. In addition, the dispersed fine skeleton-like $Cr_{23}C_6$, CrB, and Ni_3B in remelting coating can effectively prevent extend of crack and prevent the remelted coating from spalling. Compared with sprayed coating, the cohesive strength and interfacial bonding strength are obviously improved, leading to the probability of hard particles pulled out of the wear surface (λ') is lower. Hence, the wear rate (Q') of the remelted coating is smaller than that of sprayed coating.

In conclusion, the wear property of remelted coating is remarkably better than that of sprayed coating.

4. Conclusions

(1) A Ni-based thick coating with good wear resistance can be obtained by plasma spraying and remelting.

(2) After TIG remelting, the porosity decreases from 5.6% to 0.2%, and the microstructure and the compactness of the coating are improved significantly. The combining state

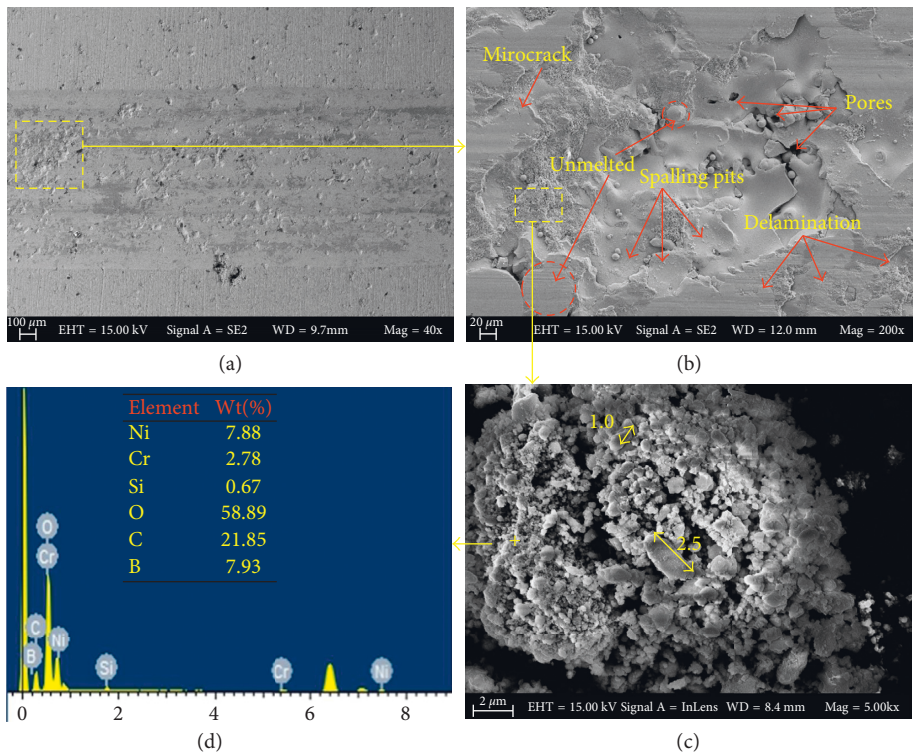

Figure 13: The sprayed coating: (a) wear scar, (b) surface wear morphology, (c) debris morphology, and (d) energy spectrum and weight percent of debris.

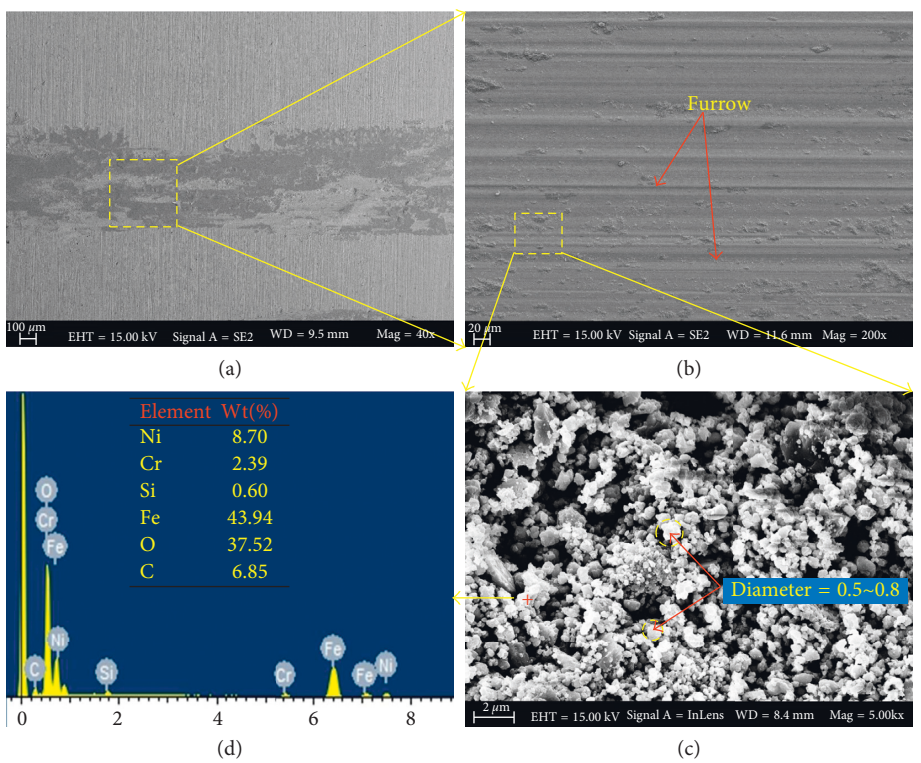

Figure 14: The remelted coating: (a) wear scar, (b) surface wear morphology, (c) debris morphology, and (d) energy spectrum and weight percent of debris.

between the coating and the substrate is changed from mechanical bonding to metallurgical bonding.

(3) After remelting, the main phases in the sprayed coating are changed from γ-Ni, Cr_7C_3, and Cr_2B to γ-Ni, $Cr_{23}C_6$, CrB, Ni_3B, and Fe_3C.

(4) The average hardness of sprayed coating is 710 $HV_{0.1}$, and its hardness is not even (580–800 $HV_{0.1}$). After TIG remelting, the average hardness of coating is 900 $HV_{0.1}$, and its hardness is uniform. The average hardness of remelted coating is increased by 26.8% compared with that of the sprayed coating.

(5) The wear resistance of remelted coating is superior than that of the sprayed coating, and the wear volume of remelted coating is only 17.1% greater than that of sprayed coating. The wear mechanism of the sprayed coating is lamellar cracking and oxidation wear, while the wear mechanism of the remelted coating is microabrasive wear and oxidation wear.

Conflicts of Interest

The authors declare that they have no conflicts of interest.

Acknowledgments

The work was financially supported by the National Natural Science Foundation of China (NSFC) under Grant nos. 51675158 and 51535011 and the Natural Science Foundation of Heibei Province of China under Grant no. E2016202325.

References

[1] J. M. Miguel, J. M. Guilemany, and S. Vizcaino, "Tribological study of NiCrBSi coating obtained by different processes," *Tribology International*, vol. 36, no. 3, pp. 181–187, 2003.

[2] Shabana, M. M. M. Sarcar, K. N. S. Suman, and S. Kamaluddin, "Tribological and corrosion behavior of HVOF sprayed WC-Co, NiCrBSi and Cr_3C_2-NiCr coatings and analysis using design of experiments," *Materials Today: Proceedings*, vol. 2, no. 4-5, pp. 2654–2665, 2015.

[3] L. Janka, J. Norpoth, and R. Trache, "Influence of heat treatment on the abrasive wear resistance of a Cr_3C_2-NiCr coating deposited by an ethene-fuelled HVOF spray process," *Surface and Coatings Technology*, vol. 291, no. 3, pp. 444–451, 2016.

[4] Z.-Y. Piao, B.-S. Xu, H.-D. Wang, and C.-H. Pu, "Effects of thickness and elastic modulus on stress condition of fatigue-resistant coating under rolling contact," *Journal of Central South University of Technology*, vol. 17, no. 5, pp. 899–905, 2010.

[5] A. Nakajima, T. Mawatari, and M. Yoshida, "Effects of coating thickness and slip ratio on durability of thermally sprayed WC ceramic coating in rolling/sliding contact," *Wear*, vol. 241, no. 6, pp. 166–173, 2000.

[6] J. Liu, R. Bolot, S. Costil, and M. P. Planche, "Transient thermal and mechanical analysis of NiCrBSi coatings manufactured by hybrid plasma spray process with in-situ laser remelting," *Surface and Coatings Technology*, vol. 292, no. 8, pp. 132–143, 2016.

[7] L. Jiangwei, W. Yan, S. Costil, and R. Bolot, "Numerical and experimental analysis of molten pool dimensions and residual stresses of NiCrBSi coating treated by laser post-remelting," *Surface and Coatings Technology*, vol. 318, no. 10, pp. 341–348, 2017.

[8] S. Zhou, J. Lei, X. Dai, J. Guo, Z. Gu, and H. Pan, "A comparative study of the structure and wear resistance of NiCrBSi/50 wt.% WC composite coatings by laser cladding and laser induction hybrid cladding," *International Journal of Refractory Metals and Hard Materials*, vol. 60, no. 32, pp. 17–27, 2016.

[9] Š. Houdková, E. Smazalová, M. Vostřák, and J. Schubert, "Properties of NiCrBSi coating, as sprayed and remelted by different technologies," *Surface and Coatings Technology*, vol. 253, no. 34, pp. 14–26, 2014.

[10] R. González, M. A. García, I. Penuelas et al., "Microstructural study of NiCrBSi coatings obtained by different processes," *Wear*, vol. 263, no. 1–6, pp. 619–624, 2007.

[11] N. Serres, F. Hlawka, S. Costil, C. Langlade, and F. Machi, "Microstructures of metallic NiCrBSi coatings manufactured via hybrid plasma spray and in situ laser remelting process," *Journal of Thermal Spray Technology*, vol. 20, no. 1-2, pp. 336–343, 2011.

[12] R. Gonzalez, M. Cadenas, R. Fernandez, J. L. Cortizo, and E. Rodríguez, "Wear behaviour of flame sprayed NiCrBSi coating remelted by flame or by laser," *Wear*, vol. 262, no. 3-4, pp. 301–307, 2007.

[13] Y. Tao, K. Sindo, and L. Zhen, "Grain refining by ultrasonic stirring of the weld pool," *Acta Materialia*, vol. 106, no. 45, pp. 144–154, 2016.

[14] G. Yi-min, *Metal Solidification Principle*, Xi'an Jiaotong University Press, Xi'an, China, 2009.

[15] W. Kurz and D. J. Fisher, *Fundamentals of Solidification*, High Education Press, Beijing, China, 2010.

[16] Z. Wen, Y. Bai, J. Yang, J. Huang, and L. Zhang, "Effect of vacuum remelting on microstructure and wear resistance of NiCrMoY coatings deposited by supersonic atmospheric plasma spraying," *Surface and Coatings Technology*, vol. 281, no. 1, pp. 62–67, 2015.

[17] S. Johansson, P. H. Nilsson, R. Ohlsson, and B.-G. Rosén, "Experimental friction evaluation of cylinder liner/piston ring contact," *Wear*, vol. 271, no. 3-4, pp. 625–633, 2011.

[18] M. Egawa, K. Miura, M. Yokoi, and I. Ishigami, "Effects of substrate bias voltage on projection growth in chromium nitride films deposited by arc ion plating," *Surface and Coatings Technology*, vol. 201, no. 3, pp. 4873–4878, 2007.

[19] L. Tong, T. Yi, S. Shuang, X. Guo, J. Lia, and D. Wang, "Continuous electron beam melting technology of silicon powder by prefabricating a molten silicon pool," *Vacuum*, vol. 143, no. 5, pp. 336–343, 2017.

[20] M. Xiangmeng, Q. Guoliang, and Z. Zengda, "Sensitivity of driving forces on molten pool behavior and defect formation in high-speed gas tungsten arc welding," *International Journal of Heat and Mass Transfer*, vol. 107, no. 7, pp. 1119–1128, 2017.

[21] X. Wang, X. Chen, Q. Sun, H.-S. Di, and L.-N. Sun, "Formation mechanism of d-ferrite and metallurgy reaction in molten pool during press-hardened steel laser welding," *Materials Letters*, vol. 206, no. 9, pp. 143–145, 2017.

[22] J. Yang, J. Han, H. Yu et al., "Role of molten pool mode on formability, microstructure and mechanical properties of selective laser melted Ti-6Al-4V alloy," *Materials and Design*, vol. 110, no. 15, pp. 558–570, 2016.

[23] A. Ohmori and C. J. Li, "Quantitative characterization of the structure of plasma sprayed Al_2O_3 coating by using copper electroplating," *Thin Solid Films*, vol. 201, no. 2, pp. 241–252, 1991.

[24] R. Colaco and R. Vilar, "Abrasive wear of metallic matrix reinforced materials," *Wear*, vol. 255, no. 1–6, pp. 643–650, 2003.